Bulletin of the New Zealand Society for Earthquake Engineering, Vol. 49, No. 3, September 2016

QUASI-STATIC CYCLIC TESTING OF EMULATIVE CAST-IN-PLACE CONNECTIONS FOR ACCELERATED BRIDGE CONSTRUCTION IN SEISMIC REGIONS

Mustafa Mashal[1], Samuel White[2] and Alessandro Palermo[3]

(Submitted *December 2015*; Reviewed *March 2016*; Accepted *April 2016*)

ABSTRACT

This paper presents findings from the first phase of testing at the University of Canterbury on seismic performance of emulative connections for Accelerated Bridge Construction (ABC) in regions of moderate to high seismicity. Emulative connections between precast concrete elements aim to target similar seismic behaviour as traditional ductile monolithic construction. The emulative solution in this research is called "High Damage Connection" (HDC).

HDCs intend to achieve similar levels of seismic performance and ductility in a precast column as that can be expected of a monolithic one. HDC relies on formation of plastic hinges in the precast column during a design level earthquake to emulate monolithic ductile behaviour.

Two types of HDCs, the grouted duct connection and member socket connection, were investigated in this research. Four half-scale precast segmental columns were constructed. Two columns featured grouted duct connections as the primary connection type. The other two columns used member socket connections. For a better understanding of the connection response under severe lateral loading, both uniaxial and biaxial testing of the columns was carried out.

In this paper, an introduction to each connection type followed by design procedure, detailing considerations and construction methodology are explained in detail. Testing results and observations of seismic performance for each connection are thoroughly presented. The research concludes that High Damage Connections have good potential for ABC in regions of moderate to high seismicity. The connections that were tested achieved good levels of energy dissipation and ductility with similar performance to conventional monolithic connections.

INTRODUCTION

The use of prefabricated elements is an effective method to achieve Accelerated Bridge Construction (ABC). For bridge substructures, the use of precast concrete components offers a number of advantages compared to conventional cast-in-place construction. The advantages include increased construction speed and quality, minimised traffic disruption, reduced life cycle costs of the structure, and increased work zone safety. Over the past several years, there has been increasing attention given to ABC in the United States, Taiwan and New Zealand. Palermo and Mashal [1] present a general background on research and implementation of ABC around the world.

In the United States, notable research into standardised precast substructure systems was carried out by Billington et al. [2]. There has also been significant interest in ABC for bridge substructure systems by the Federal Highway Administration [3] and several State Departments of Transportation (DOTs), including Washington DOT [4], Texas DOT [5], and Utah DOT [6].

There have been several applications of ABC in the United States in regions of low seismicity. Examples include precast segmental piers on US 183 and precast pier cap on US 290 (Figure 1a) in Austin, and more recently the precast hammer head caps in Bell County on US 36 over Lake Belton (Figure 1b) in Texas. Another example of the precast pier is Edison Bridge (Figure 1c) on US 41 in Fort Myers, Florida. However, application of ABC in regions of moderate and high seismicity has been limited, mainly due to concerns regarding the seismic performance of connections between precast elements [7].

The need for improved seismic performance of precast structures was highlighted during the Loma Prieta (1989) and Northridge (1994) earthquakes by Buckle [8] and Hawkins et al. [9]. During the late 1990s, there was little research done on precast bridge piers in seismic regions. One example is Mander and Cheng [10].

Marsh et al. [11] presents concepts and summary of the latest research for several types of connections which can be used for prefabricated substructures in regions of moderate to high seismicity. These connections are classified as emulative and non-emulative, depending on whether they emulate the seismic behaviour of conventional monolithic connections, or improve on the seismic performance - often through the use of jointed, rocking systems or other advanced methods. The connections are compared in terms of technological readiness, potential seismic performance, and time savings potential.

Emulative cast-in-place connections for ABC substructures include the use of bar couplers [12] and [13], grouted duct connections [14], [15], and [16], pocket connections [15], and member socket connections [17]. Non-emulative cast-in-place connections for ABC include segmental post-tensioned rocking piers [18] and [19], hybrid or dissipative controlled rocking connections [20], [21], and [22], and some emerging technologies [23].

[1] *Corresponding Author. Senior Structural and Earthquake Engineer, Silvester Clark Consulting Engineers, formerly PhD Candidate, University of Canterbury, Christchurch, mmashal@buffalo.edu (Member)*

[2] *Bridge Engineer, Opus International Consultants, formerly Master's of Engineering Student, University of Canterbury, Christchurch*

[3] *Associate Professor, University of Canterbury, Christchurch (Member)*

The research at the University of Canterbury is part of a project titled "Advanced Bridge Construction and Design for New Zealand" (ABCD), funded by the Natural Hazards Research Platform (2011-2015). The research aims to experimentally investigate the seismic performance of emulative and non-emulative precast connections. These connections are developed for prefabricated bridges with short-to-medium spans (up to 30 meters). A range of connection types are investigated. They are characterised as either "High Damage" "Controlled Damage" [24] or "Low Damage" [25] connections, with each category corresponding to the type and extent of damage that can be expected during an earthquake.

(a) US 290, Texas

(b) US 36, Texas

(c) US 41, Florida

Figure 1: Recent examples of ABC for precast substructure and superstructure systems in low seismic regions of the United States.

This paper focuses on the use of High Damage connections (also known as emulative connections) for bridge substructures - in particular column-footing connections. High Damage connections are designed to emulate the performance of conventional monolithic connections, while offering the advantages associated with prefabrication. They are termed "High Damage" as they are detailed such that plastic hinges form in the structure under a design level earthquake, resulting in a relatively high amount of damage when compared to most non-emulative connection types. The formation of plastic hinges results in spalling of concrete and yielding of reinforcing bars. In extreme cases, bar buckling or fracture may potentially require repair or replacement of sections of the bridge or the bridge as a whole following the earthquake.

The first phase of testing investigated seismic performance of two variations of High Damage connections. Four half scale precast segmental piers were tested under quasi-static uni and bi-directional loading. Two specimens with square cross-section featured Grouted Duct Connections (GDC) for the column to foundation connection. The other two specimens had circular cross-sections with Member Socket Connections (MSCs) for the column to foundation connection. The segment to segment connection in all piers was GDC.

PROTOTYPE STRUCTURE AND SPECIMENS

Four half-scale specimens were developed based on the prototype bridge structure shown in Figure 2. The prototype structure is a representation of typical highway bridge stock in New Zealand. The bridge has six spans of equal length (12 m) and has dimensions shown in Figure 2. The height from top of the footing to centre of gravity of the bridge was taken to be 5 m (Figure 2b). Note the footings shown in Figure 2 are indicative only.

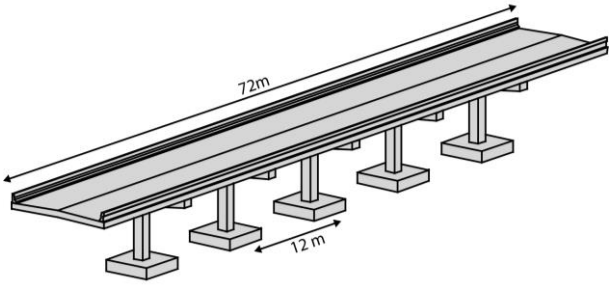

(a) Longitudinal profile

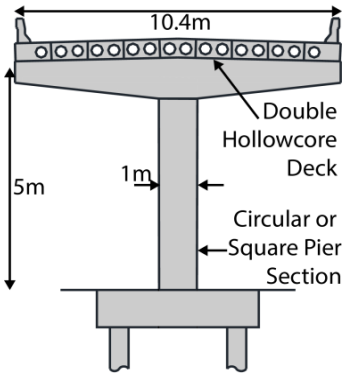

(b) Transverse elevation

Figure 2: Prototype bridge.

Both circular and rectangular pier cross section shapes are considered for the prototype structure. The superstructure is a double hollow-core deck with a beam depth of 587 mm in accordance with the New Zealand Transport Agency (NZTA) Report 364 "Standard Precast Concrete Beams" [26]. The

report presents four types of precast girder systems (Single and double hollow-cores, I-beam, and T-section) for construction of bridges up to 30 m in span.

A force-based design procedure from NZTA Bridge Manual (2nd Edition) [27] and New Zealand Standards 1170.5 "Earthquake Actions" [28] was used to determine the design lateral loads for the prototype. The bridge is assumed to be situated on non-liquefiable soil. The footings are assumed to be fully fixed and no soil-structure interaction is taken into account. Since the High Damage connections are designed to emulate the seismic performance of conventional monolithic construction, similar effects of soil-structure interaction and foundation flexibility would be expected, had they been considered. Consideration of foundation flexibility would result in increased fundamental period of the structure, with reduced base shear demands and larger displacement demands in seismic events.

The axial loads used in the design and testing of the columns were based only on the self-weight of the column and the dead load of the bridge deck with no additional vehicle loading in accordance with Load Combination 3A given in Table 3.2 of the Bridge Manual [27].

When calculating the elastic period of the bridge, cracked section properties of the columns was taken into account. The gross moment of inertia was factored by 0.3 to account for the cracked section. The elastic period of the bridge was calculated to be less than 0.4 sec, using a simple single degree of freedom approach.

According to NZS 1170.5 [28], based on a hazard factor of 0.3 (high seismicity), soil class C (Shallow Soil), return period of 1000 years and an assumed ductility of 3.0, the seismic coefficient was calculated to be 0.37. This results in base shear and moment demands of 170 kN and 425 kNm, respectively, for a typical half-scale specimen with square section. A base shear of 145 kN and moment demand of 375 kNm was used for the specimens with circular cross sections. The yield displacement in accordance to NZS 1170.5 was calculated to be approximately 11 mm or 0.45% drift ratio. Using a ductility of 3.0, the ULS displacement is estimated to be 33 mm or approximately 1.4% drift ratio from force-based design.

The specimens and connection types are listed in Table 1 and material properties are summarised in Table 2.

Table 1: Summary of High Damage specimens.

Specimen ID	Primary Connection Type	Column Section	Testing Protocol
HDS1	Grouted Duct	Square	Uniaxial
HDS2	Grouted Duct	Square	Biaxial
HDC1	Member Socket	Circular	Uniaxial
HDC2	Member Socket	Circular	Biaxial

Table 2: Summary of material properties.

Material	Specified Strength (MPa)	Tested Strength (MPa)			
		HDS1	HDS2	HDC1	HDC2
Concrete	40	60	51	48	44
Steel (Longitudinal)	500	516	516	516	516
Steel (Transverse)	500	556	556	556	556
Grout	40	65	38	58	44

TESTING METHODOLOGY

The uniaxial testing arrangement is illustrated in Figure 3a. This type of testing represents seismic loads on the bridge pier in the transverse direction. In this case, it is assumed that lateral loads in the longitudinal direction of the bridge are resisted by the abutments. During testing, this was represented by using a lateral ram with 400 kN capacity acting on one of the horizontal directions (North-South) on the specimen. The ram was attached to a reaction steel braced frame as shown in Figure 3a.

An unbonded post-tensioned bar was used to apply axial load representing the dead load of the superstructure (Figure 4a). The bar tension was regulated to apply a relatively constant axial load throughout testing.

The uniaxial quasi-static loading protocol consisted of three cycles at each drift limit followed by a smaller cycle, with consecutive drift limits increasing by a factor of 1.2 to 1.5. The loading protocol was adopted from ACI-ITG1 [29] and is plotted in Figure 3b.

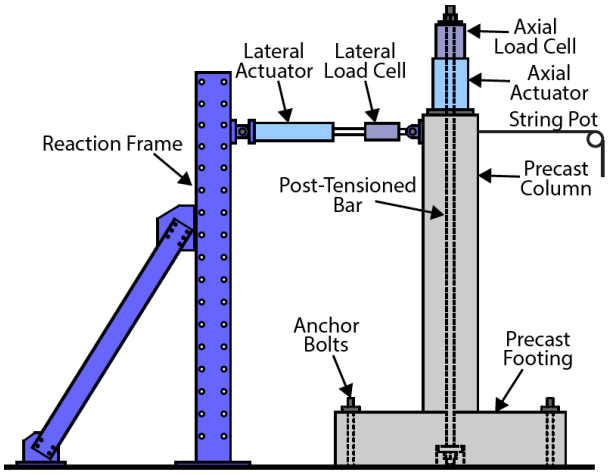

(a) Elevation view

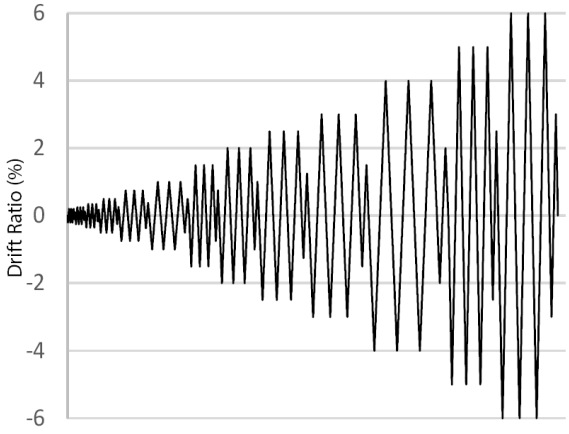

(b) North/South (NS) drift input

Figure 3: Uniaxial testing details.

The biaxial testing arrangement is shown in Figure 4b and Figure 5a. The biaxial loading protocol used in this testing was adopted from Marriott [30] and Muir et al. [31]. The biaxial quasi-static loading protocol consisted of cycles of uni-directional push and pull in the East-West (EW) direction (Figure 5b), followed by the North-South (NS) direction (Figure 5c), before simultaneously loading both directions resulting in a clover shaped drift path as shown in Figure 5d.

Using clover shape testing protocol can be a conservative approach for testing of bridge piers. In real life, bridge piers are not normally subjected to 100% seismic demand in both longitudinal and transversal directions simultaneously. For bridge piers, it is common that seismic loads acting in the transversal direction govern the design of piers.

(a) Typical column test setup under uniaxial loading

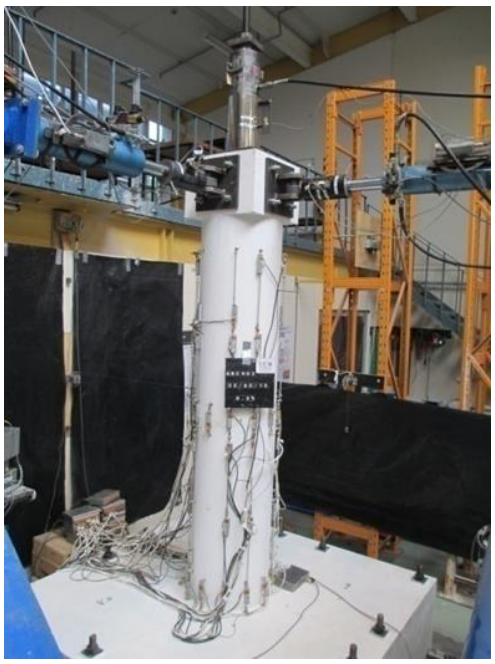

(b) Typical column test setup under biaxial loading

Figure 4: Testing arrangements.

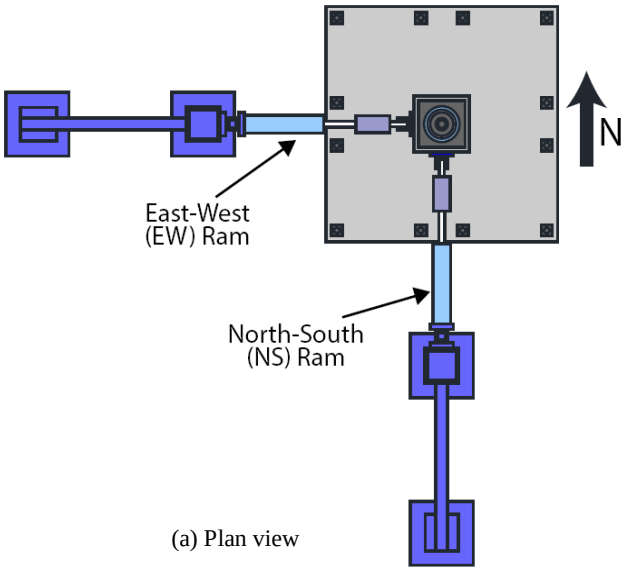

(a) Plan view

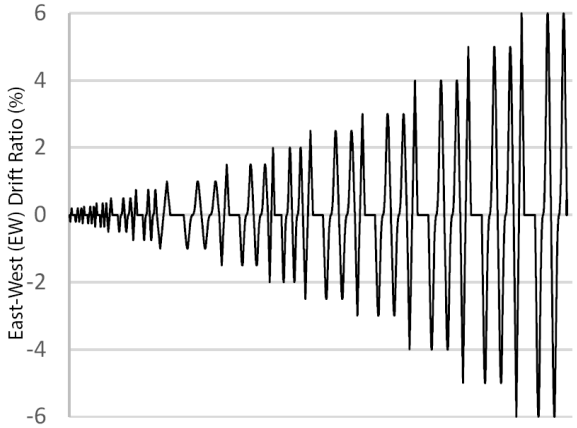

(b) East/West (EW) drift input

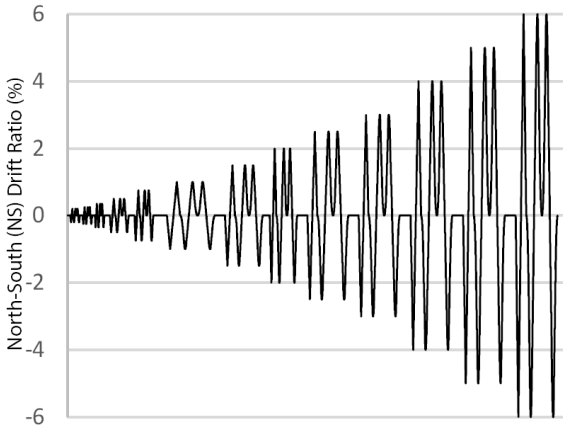

(c) North/South (NS) drift input

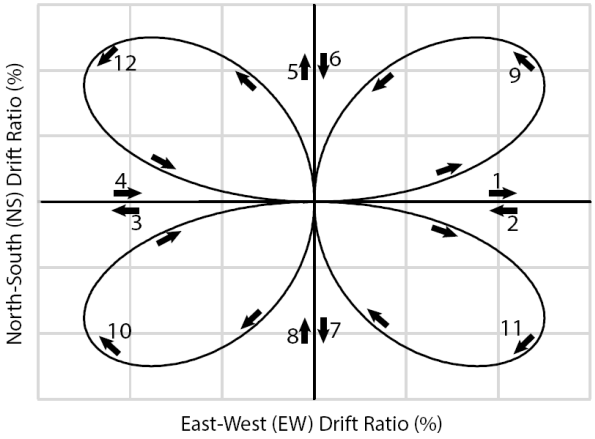

(d) Biaxial loading sequence

Figure 5: Biaxial testing details.

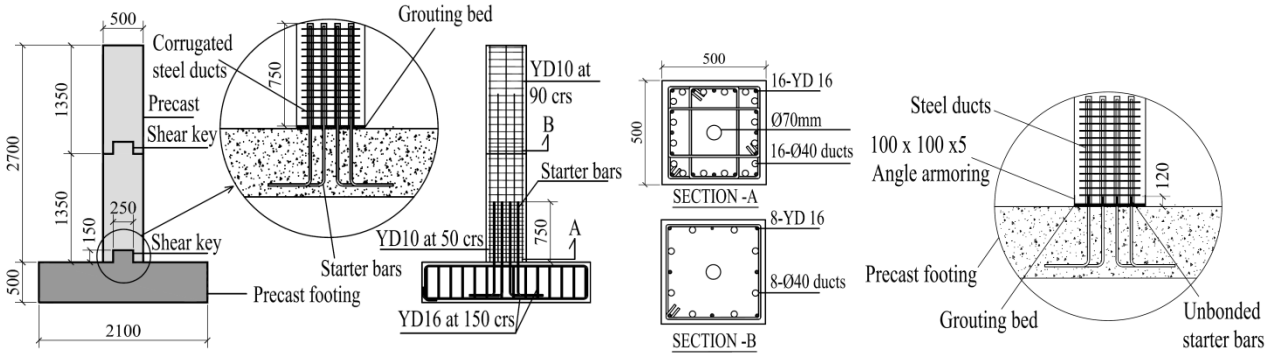

a) Elevation and reinforcing detailing of HDS1 and HDS2 (b) Segment sections (c) HDS2 base connection

Figure 6. HDS1 and HDS2 reinforcing details.

GROUTED DUCT CONNECTION (GDC)

In the Grouted Duct Connection (GDC), starter bars extending from one precast element are inserted into ducts which are cast into a second element. Grout is pumped into the ducts through external tubes after assembly of the elements, which secures the connection.

GDC can be used for pile to pile cap, spread footing or pile cap to column, column to cap beam, and splices between the column segments or cap beam segments [11]. Previous experimental testing on GDC include Matsumoto et al. [14], Brenes et al. [16], Riva [32], Culmo [13], Matsumoto [15], and Restrepo et al. [33]. The GDC is generally used in capacity protected regions of the structure where the elements are likely to remain elastic.

Design and Detailing Considerations: HDS1 and HDS2

All columns in this research were designed in accordance with New Zealand Standards 3101 "The Design of Concrete Structures" [34]. The reinforcing details for HDS1 and HDS2 were identical, as shown in Figure 6. A total of 16-YD16 longitudinal bars were located at the lower connection while 8-YD16 bars were used at the upper connection (Figure 6b).

The corrugated steel ducts were 40 mm in internal diameter and were cast into the base of each column segment. The steel ducts were fabricated from 0.30 mm thick hot-dipped galvanised strip steel. YD10 stirrups at 50 mm spacing were used to provide confinement and shear resistance in the plastic hinge regions of the column, as shown in Figure 6a. A stirrup spacing of 90 mm was used outside the plastic hinge regions.

For HDS2, the design featured some improved detailing for the column to footing connection. The first improvement was addition of armouring at the base of the column to protect against spalling damage at the connection interface (Figure 6c). The armouring consisted of 100x100x5 mm Angle located around the bottom edges of the lower column segment. A simple approach was adopted for design of the armouring using the confined concrete model by Mander et al. [35]. More detailed approaches including Finite Element Modelling could also be used.

The second improvement was debonding of the longitudinal starter bars over a length of 120 mm to reduce strain concentration effects at the connection interface. Normal duct tape was used to wrap the 120 mm length of the starter bars. However, when considering the durability of the connection, Denso Tape would offer better corrosion resistance. The 120 mm unbonded length was determined based on observation from the testing of HDS1 in which there was no debonding of starter bars at the column to footing interface resulting in a shorter plastic hinge than would be expected from a monolithic connection. The improvements in connection detailing for GDC were intended to increase the ultimate ductility and displacement capacities of the column.

A 2.1 meter square footing with depth of 500 mm was used at the base of the columns which was fixed to the floor using hold-down bolts.

Shear keys were located at the column to footing and segment to segment connections to transfer the shear loads across the connection interface. Although shear force can be resisted through the dowel action in the starter bars, it was preferred in this case that the shear keys transfer all shear loads across the interface. In this case, the starter bars were intended to contribute during flexural action only, with shear transfer through dowel action neglected. The shear keys were designed using the principals of shear friction according to NZS 3101 [34]. It was thought that the use of shear keys would minimise shear degradation in the connection during cyclic loading. In past research studies [11], shear friction and dowel action of reinforcing bars were relied on to transfer the shear forces across the connection interface.

A 70 mm diameter duct was located at the centre of the column and footing to house the unbonded post-tensioned bar which simulated dead on the column. The bar was fixed using mechanical anchorages at each end.

Load transfer mechanisms under gravity and lateral loads in a typical GDC are illustrated in Figure 7a and Figure 7b, respectively. Shear is transferred across the GDC through a combination of friction and bond in the grouted interface, and bearing of the column against the shear key.

Figure 7c shows the primary bond mechanism in the corrugated ducts where tension loads in the column are transferred to the starter bars extending from the footing. The primary load transfer mechanism in the duct is through bearing of the deformations of the corrugated duct and reinforcing bar against the surrounding grout and concrete. Only a small amount of stress is transferred through chemical adhesion and friction between the steel and surrounding concrete or grout as previously studied by Brenes et al. [16] and Raynor et al. [36]

Due to increased bond inside the corrugated ducts, a lower length of strain penetration of the reinforcing bars occurs at the connection interface than in monolithic connections. During lateral displacement, the largest cracks occur at the interface of the column and footing which leads to strain concentrations in the bar at the connection interface as presented by Raynor et al. [36]. This is illustrated by Line A in Figure 7d.

Strain concentration reduces the ductility capacity of the bar and makes it susceptible to low cycle fatigue failure.

Debonding of starter bars over a certain length at the connection interface helps to mitigate the effect of strain concentration by spreading the total elongation of the bar over a longer length. Thus, it reduces the peak strain in the bar as previously studied by Mander et al. [37], Kawashima et al. [38], and Stanton et al. [21]. This is illustrated by Line B in Figure 7d. Bar debonding has also been shown to result in less concrete spalling and improved ductility for the column.

A more accurate method for determining the required debonded length is to consider the connection as a rocking interface where sufficient debonded length is provided to limit the strain in the reinforcing bars to less than 5% [39].

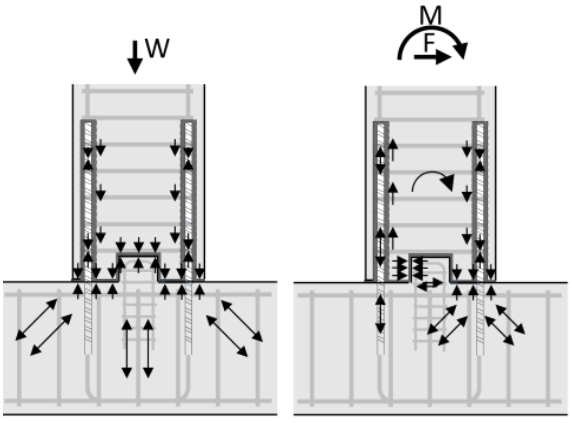

(a) Gravity transfer in GDC (b) Lateral loads in GDC

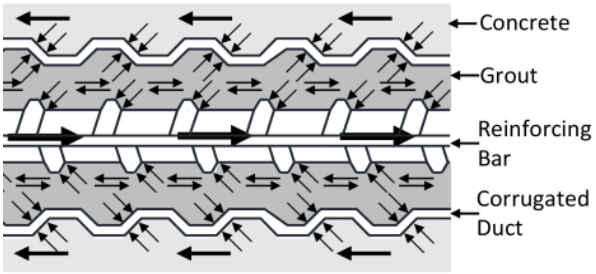

(c) Bond mechanism in duct

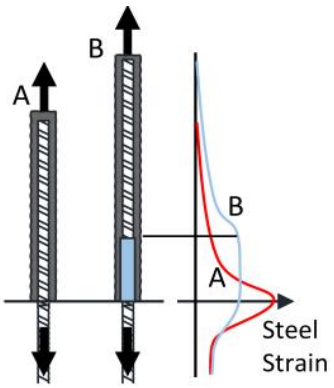

(d) Strain distribution

Figure 7. Load transfer mechanism in GDC.

All elements in this research were constructed in a precasting yard (Bradford Precast Ltd.) in Ashburton, New Zealand. Figure 8 provides photos from construction and assembly of HDS1 and HDS2. A plywood template was used to ensure good alignment of the starter bars and the corrugated ducts between the segments during precasting. The precast elements were subsequently transported to the Structures Laboratory at the University of Canterbury where they were assembled and grouted. Grouting of the starter bars was done by an expert contractor (BBR Contech) to ensure good quality of the connections.

Test Results: HDS1 and HDS2

For HDS1, the column to footing joint started cracking at a drift of 0.35%. Most of the cracks up the height of the column remained less than 0.4 mm in width during testing. There were only 3 large cracks at the column plastic hinge zone at the base. The largest crack was located at the column to footing interface.

Spalling of concrete occurred during cycles of 3% drift ratio which corresponded to Ultimate Limit State (ULS) performance level (Figure 9a). Following testing (Figure 9b), spalling had occurred up to a height of 250 mm from the base of the column. The plastic hinge length was taken as the spalling height at the column base which was measured using

Figure 8. Construction and assembly of HDS1 and HDS2.

a measuring tape following testing. Further research is needed on measuring the actual plastic hinge length for this type of connection.

Failure and buckling of the footing starter bars occurred during the first cycle of the 5% drift ratio which corresponded to Maximum Considered Earthquake (MCE) performance level (Figure 9b). Buckling of starter bars occurred between the first stirrup in the column and the top of the footing. This distance was approximately 60 mm, as shown in Figure 9b. Given the 25 mm grouting bed (made of Sika 212) underneath the column and 35 mm concrete cover for the precast column, it was difficult to have the first stirrup in the column placed closer than 60 mm from top of the foundation. The distance between other stirrups in the plastic hinge zone was 50 mm.

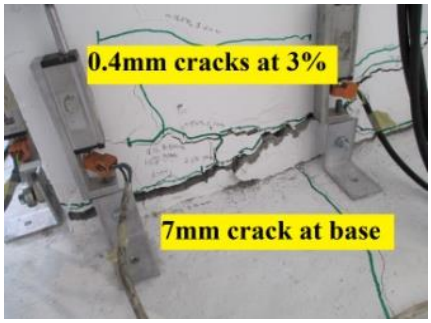

(a) Concrete spalling, HDS1

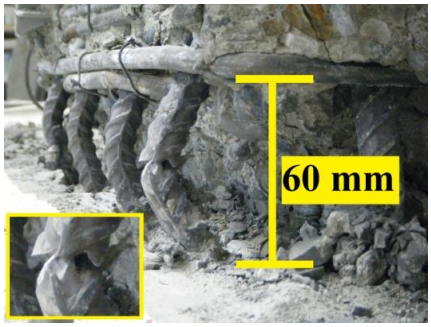

(b) Plastic hinge, HDS1

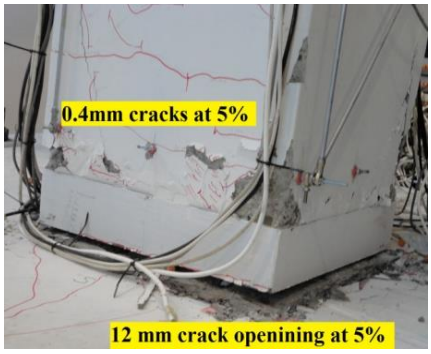

(c) Spalling and rocking, HDS2

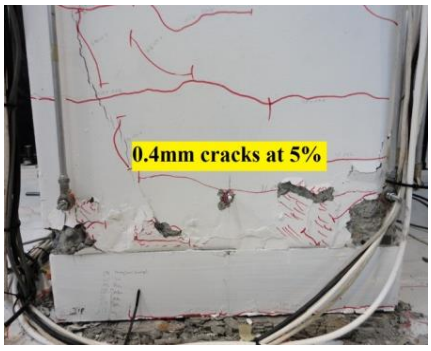

(d) Plastic hinge, HDS2

(e) HDS1 after testing

(f) HDS2 after testing

Figure 9. Testing photos of HDS1 and HDS2 with GDC.

For HDS2, cracks started forming during cycles of 0.25% drift ratio. The armouring was effective at limiting spalling in the column. The majority of minor spalling occurred around the corners of the column during cycles of 2.5% ratio (3.25% resultant drift, ULS performance level) at the clover loading stage. During testing, there was only one large crack located at the column to footing interface. This crack was measured to be

12 mm during cycles of 5% drift ratio (Figure 9c). The majority of other cracks at this drift ratio (5%) were only 0.4 mm in width. There was severe flaking of the grouting bed on top of the footing during 5% drift ratio as can be seen in Figure 9c.

In general, the performance of HDS2 was similar to that of HDS1, despite being subjected to biaxial loading. By the end of testing, minor spalling had occurred up to a height of 250 mm from the base of the column which was mainly concentrated at the corners (Figure 9d). Bar failure occurred during the 5% drift cycle (6.5% resultant drift, MCE performance level) which was larger than the failure point of the HDS1 column. This indicated that debonding of the starter bars over 120 mm length was effective in limiting the longitudinal steel strains, thus increasing the ultimate displacement capacity of the column.

Figure 9e and Figure 9f present the extent of damage in HDS1 and HDS2 following testing, respectively.

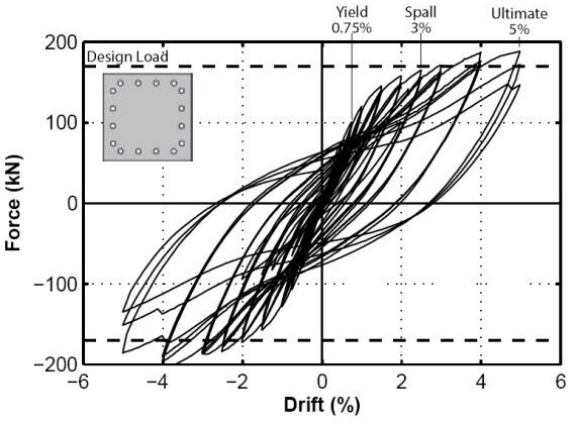

(a) HDS1

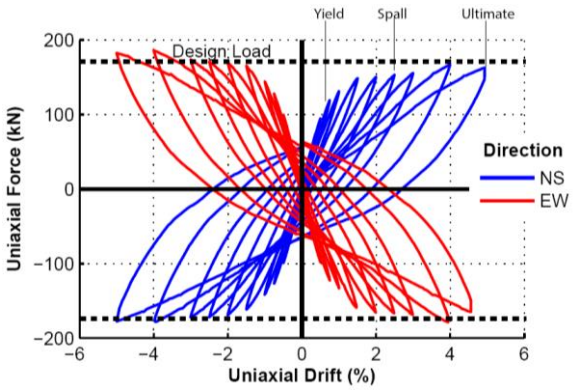

(b) HDS2 (uniaxial)

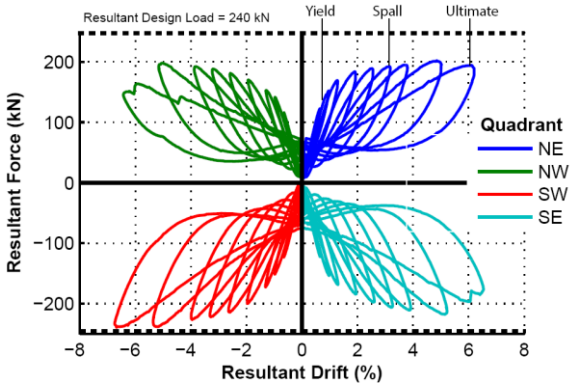

(c) HDS2 (resultant biaxial)

Figure 10. Force-Drift hysteresis plots for HDS1 and HDS2.

Figure 10 presents force-drift hysteresis plots for HDS1 and HDS2. Both specimens showed stable response. The post-yield stiffness increase in HDS1 (Figure 10a) was due to a construction error. Upon disassembly of the column, it was found that the grout had flowed into the central duct during grouting of starter bars for the top segment. This caused the unbonded post-tensioned bar to become fully bonded. This means that the post-tensioned bar was behaving as reinforcing bar which had led to an increased post-yield stiffness as the bar load increased with increasing drift. This was considered to affect the capacity of the section, but not the overall ductility and performance of the column, as longitudinal bar rupturing was achieved at 5% drift ratio. Figure 10b and Figure 10c present the uniaxial and biaxial (resultant clover) plots for HDS2, respectively.

Acceleration-Displacement Response Spectrum (ADRS) curves are plotted in Figure 11 to present the expected seismic performance of each column for various hazard levels from NZS 1170.5 [28] using a structural performance factor (S_p) of 1.0 in accordance with Marriott [30].

The elastic design spectrum is converted into ADRS using the displacement-based methodology presented in Priestley et al. [43] which is based on an assumed sinusoidal harmonic oscillation theory. In this approach, to normalize the capacity curve, the base shear and displacement from the backbone curve are divided by the weight of the half-scale prototype bridge and the height of the test column, respectively.

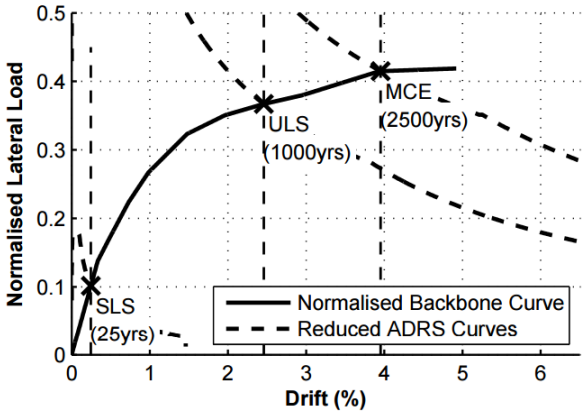

(a) HDS1 (North/South Direction)

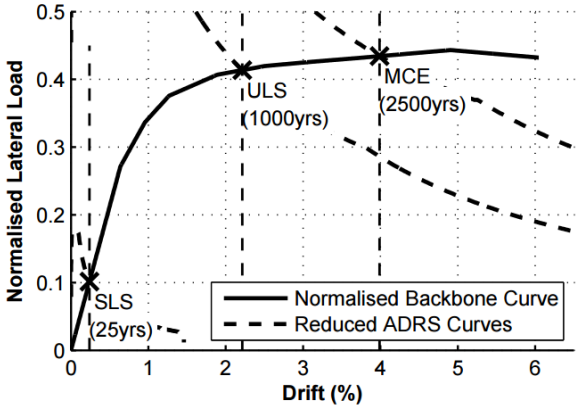

(b) HDS2 (North/South Direction)

Figure 11. Acceleration-Displacement Response Spectrum (ADRS) curves for HDS1 and HDS2.

The spectral acceleration (S_a) for a given demand is reduced by a factor (η) calculated in accordance with Priestley et al. [43] (refer to Table 3). η is calculated using the area-based damping ($\xi_{area\text{-}based}$) which is calculated from the experimental

hysteresis plot. The area-based and elastic damping are converted into an Equivalent Viscous Damping (EVD, ξ_{eq}). EVD is taken as the sum of the corrected area-based hysteretic damping (ξ_{hyst}) and the elastic tangent damping ($\xi_{el,\ tangent}$). A time-history calibration factor is also applied to EVD to account for dynamic effects. The spectral accelerations (S_a) were normalised by dividing by the acceleration of gravity. The spectral displacement (S_d) for each ADRS curve were normalised by dividing by the height of the test column.

Table 3: ADRS reduction factors for HDS specimens.

		HDS1		HDS2	
Limit State	**Return Period**	**Corrected EVD**	**η**	**Corrected EVD**	**η**
SLS	25	5.0%	1.0	5.0%	1.0
ULS	1000	9.4%	0.79	8.6%	0.81
MCE	2500	16%	0.63	15%	0.64

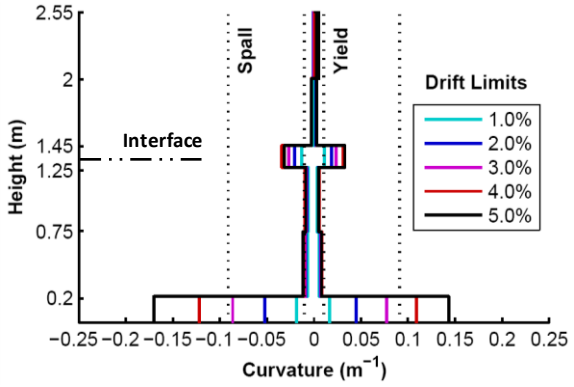

(a) HDS1 (North/South Direction)

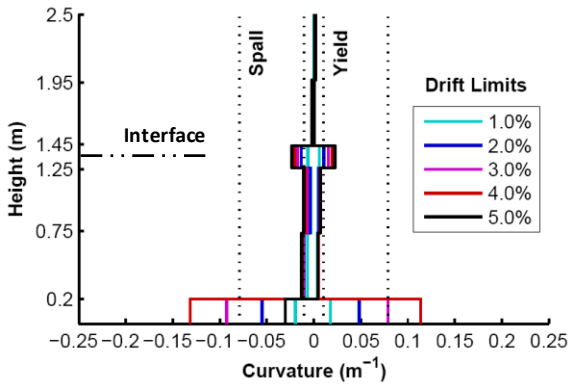

(b) HDS2 (North/South Direction)

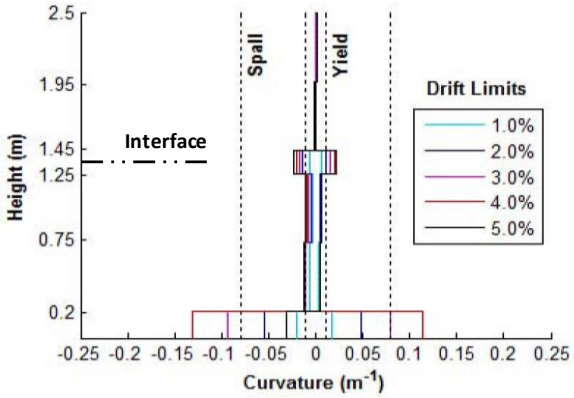

(c) HDS2 (East/West Direction)

Figure 12. Curvature distribution for HDS1 and HDS2.

The increased initial stiffness of HDS2 in Figure 11b compared to HDS1 (Figure 11a) was due to debonding of starters bars and base armouring which resulted in less distributed cracking up the height of the column.

Curvature distribution up the height of each column is shown in Figure 12. Curvature was measured using an array of potentiometers mounted to the faces of the test columns. An alternative method could be to place several marks (dots) on the specimen before testing, then capturing the movements of dots using a camera when the specimen is being pulled or pushed. Other methods may include the use of advanced sensors and instruments which could provide improved measurement of the curvature.

In the Figure 12 plots, it can be seen that a second plastic hinge formed at the segment to segment interface. During testing there was slight opening of the segment to segment joint in both specimens. However, after cycles of 1% drift ratio, the majority of the damage and gap opening was concentrated at the column to foundation interface. The strength of the upper joint could be increased to avoid gap opening at this location, if desired. There may be potential benefits to allowing multiple plastic hinge locations along the column member, but further validation through experimental testing (particularly dynamic testing) is required.

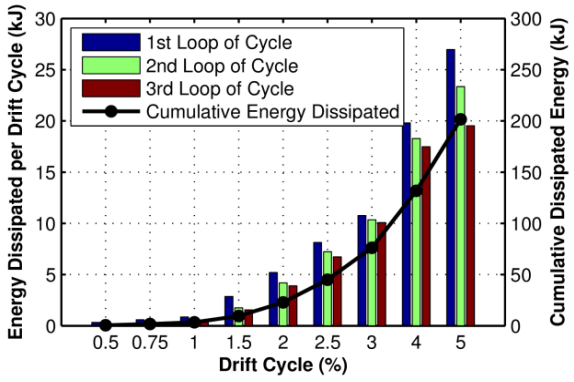

(a) HDS1

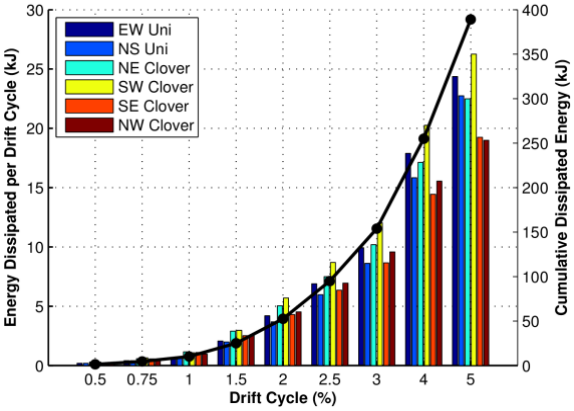

(b) HDS2

Figure 13. Dissipated energy for HDS1 and HDS2.

The amount of energy dissipated per cycle for each column is plotted in Figure 13. The dissipated energy was calculated using a numerical integration of the area enclosed inside the hysteresis loop for each of the first three cycles at each drift ratio. The cumulative dissipated energy is the sum of the energy dissipated in the three cycles at each drift ratio and is shown by black lines in Figure 13. The equivalent drift input of the uniaxial testing for HDS1 was applied through both lateral rams during the biaxial testing of HDS2. Thus, the

cumulative dissipated energy for HDS2 was almost double that of the HDS1 column (Figure 13).

MEMBER SOCKET CONNECTION (MSC)

The Member Socket Connection (MSC) is formed by embedding a precast element inside another element which can be either precast or cast-in-place. If both elements are precast, grout or concrete is poured into the gap between the elements bonding them together. The other option is to have the second element cast around the first one [11]. The second option offers the advantage of increased tolerance in the placement of the column element in the socket, but requires more on-site concrete pouring which can slow the construction process.

MSC can be used for footing to column, column to cap beam, and pile to pile cap connections [11]. The research at the University of Canterbury considered MSC for the column to footing connection.

These connections have been used in the building industry, but there are a few records of their use in bridge structure as presented in Marsh et al. [11]. Recently, this type of connection was used for footing to column connection of a precast pier on Interstate Highway 5 in the State of Washington [40]. The connection was previously investigated and experimentally tested by Haraldsson et al. [40] at the University of Washington in Seattle. More details on socket connections can be found in Riva [32] and Marsh et al. [11].

Design and Detailing Considerations: HDC1 and HDC2

Both circular section columns were identical with reinforcing details shown in Figure 14. Similar to HDS1 and HDS2 the segment to segment connection was a GDC in both cases.

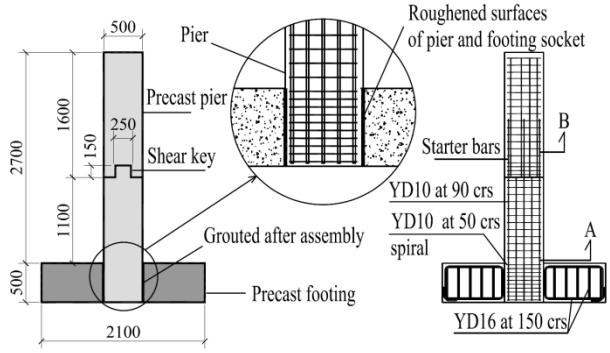

(a) Elevation and reinforcing detailing of HDC1 and HDC2

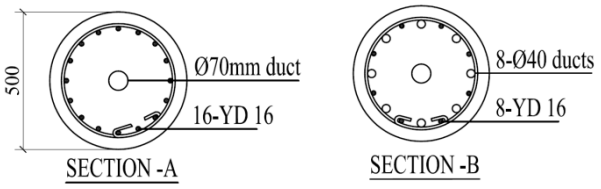

(b) Segment sections

Figure 14. HDC1 and HDC2 reinforcing details.

A 2.1 meter square footing with a depth of 500 mm was used. The footing was reinforced using a top and bottom grid of YD16 bars at an average spacing of 150 mm. A socket of 500 mm depth and 520 mm diameter was used to support the column. The socket walls and concrete surface of the portion of the column inside the socket (stub) were roughened during the prefabrication process. The roughened surface was made by applying a retarding agent to the formwork before casting the concrete. After the formwork was removed (generally 1-2 days after casting), water blasting was used to expose the aggregate on the concrete surface. When pouring the grout to fill the void during the assembly process, the roughened surface provides a better bond of the surface with the layer of grout.

Sufficient socket depth is required for the loads from the column to be effectively transferred to the footing. Shear and bearing loads must be transferred through the grouted interface between the column and footing as shown in Figure 15a. Lateral loads also contribute to shear in the grouted interface as described by Osanai et al. [41] and illustrated in Figure 15b. Inadequate socket depth may result in shear failure of the grouted interface which can initiate a punching shear failure in the footing [11].

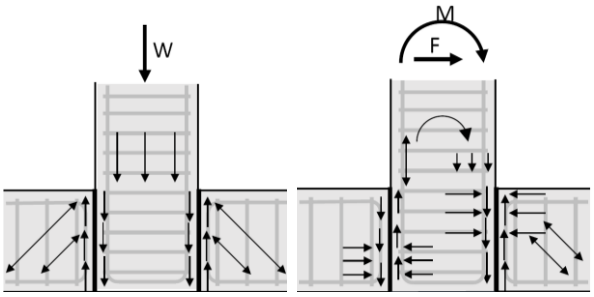

(a) Gravity transfer (b) Lateral loads transfer

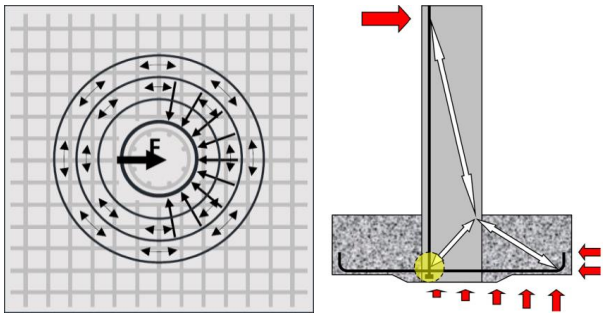

(c) Hoop stresses around socket (d) Strut and tie model [40]

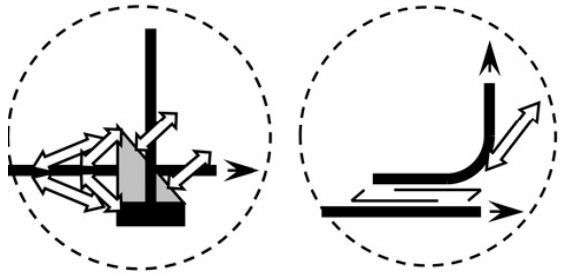

(e) Headed bar (f) Bent-out bar

Figure 15. Detailing considerations for MSC.

The bearing stresses induced in the footing by lateral loads are shown in Figure 15c. It is shown that accompanying the compressive stresses in the radial direction are hoop tensile stresses that lie at a perpendicular direction. The tensile stresses cause radial cracking which originates at the socket and propagates to the perimeter of the footing. This can be mitigated by providing circular hoops or straight bars in the footing orientated tangentially to the hoop stresses.

A strut and tie model proposed by Haraldsson et al. [40] for MSC is presented in Figure 15d. According to this model, if a headed bar detail is used (Figure 15e), the diagonal strut force within the column is transferred to the column reinforcing bars through a node which is comprised of three compression struts. The force transfer in this case is dependent on direct bearing. In contrast, in a conventional bent-out bar detail (Figure 15f), internal forces are transferred through the bond

Figure 16. Construction and assembly of HDC1 and HDC2.

to the curved part of the reinforcing bar. Therefore, it is recommended that a headed bar detail is used to provide a more direct transfer mechanism of internal forces in MSC.

Sufficient gap must be left between the column and footing to allow for tolerance when assembling the precast elements, and to allow for the flow of grout when pouring the joint. The gap should not be too large since this will reduce the effectiveness of the grout interface to transfer shear between the elements [41].

Figure 16 presents photos from construction and assembly of HDC1and HDC2. The roughened surface of the column stub can be noticed.

Test Results: HDC1 and HDC2

For HDC1, the column started cracking during cycles of 0.25% drift ratio. The cracking continued throughout testing up the height of the column. There was a larger distribution of thick cracks (more than three) at the base of the column, indicating a longer plastic hinge length than observed in HDS1 and HDS2 (Figure 17a).

The plastic hinge length was taken as the spalling height in the column which was measured to be equal to the depth of the section (500 mm). This is the same plastic hinge length as given by NZS 3101 [34] for uni-directional plastic hinges in a ductile monolithic column (equal to the diameter of the column). Further research is required to quantify the plastic hinge length for MSC.

Minor spalling initiated during cycles of 3% drift ratio (Figure 17a). During the 6% drift cycle, the lateral actuator hit the stroke limit at the pulling stage of the cycle, meaning a drift in the South direction of only 5.2% could be achieved. Following testing, spalling had occurred up to a height of 500 mm from the base of the column (Figure 17b). Reinforcing bar rupture occurred during the peak of second cycle at 6% drift.

For HDC2, the cracking pattern and overall behaviour was similar to that of HDC1. However, the spalling was much more significant than that observed in testing of HDC1. The spalling had extended all around the base of the column (Figure 17d). Figure 17e and Figure 17f present the extent of damage in HDC1 and HDC2 following testing, respectively.

Experimental results showed stable hysteresis loops for both columns. The columns achieved good levels of ductility and strength. From the Figure 18 plots, strength degradation under cyclic loading at larger displacements can be observed.

ADRS curves are plotted in Figure 19 with reduction factors summarised in Table 4. It can be seen that a ULS seismic hazard (1 in 1000 years) generates just under 3% of drift in the columns which was the value adopted for the force-based design of the prototype structure. This indicates that good assumptions were made during the design process of the columns with member socket connection.

Table 4: ADRS reduction factors for HDC specimens.

		HDC1		HDC2	
Limit State	**Return Period**	**Corrected EVD**	**η**	**Corrected EVD**	**η**
SLS	25	5.0%	1.0	5.0%	1.0
ULS	1000	7.8%	0.85	7.8%	0.85
MCE	2500	18%	0.60	16%	0.62

The post-yield stiffness of the columns is lower than that seen in the HDS1, indicating that the unbonded post-tensioned bar performed as desired in simulating the constant axial load on the column during testing.

Similar to HDS1 and HDS2, a second plastic hinge was located at the segment to segment joint in both columns (Figure 20).

The cumulative dissipated energy for HDC2 was less than double of that for the HDC1 (Figure 21). This is likely to be due to the higher level of damage sustained by the column during testing.

Figure 22a presents the hysteretic damping plot for each test specimen. For comparison, theoretical hysteretic damping curves for Takeda-Thin and Takeda-Fat models (which represent the reasonable range for reinforced concrete structures) based on Dwairi-Kowalsky damping [42] and in accordance with Priestley et al. [43], are also plotted alongside the experimental hysteretic damping. For the theoretical damping curves, it was assumed that the system had an effective period (T_{eff}) equal to or greater than 1.0 second.

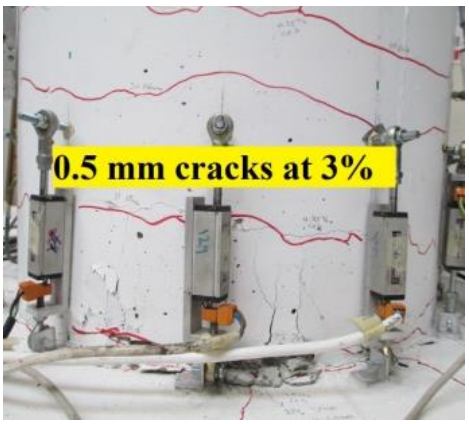

(a) Concrete spalling, HDC1

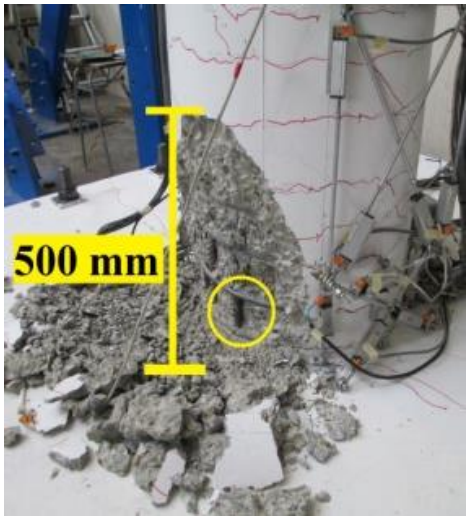

(b) Plastic hinge, HDC1

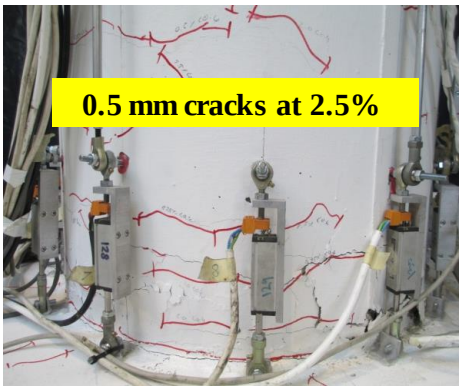

(c) Concrete spalling, HDC2

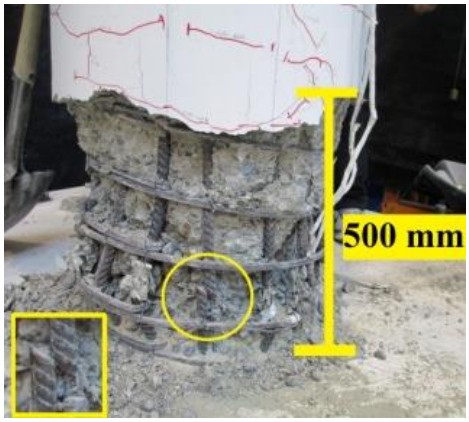

(d) Plastic hinge, HDC2

(e) HDC1 after testing

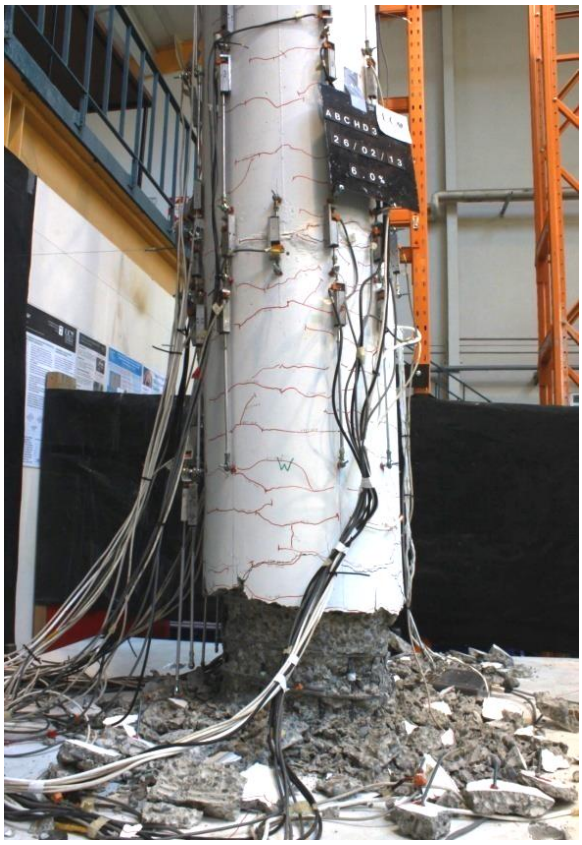

(f) HDC2 after testing

Figure 17. Testing photos of HDC1and HDC2 with MSC.

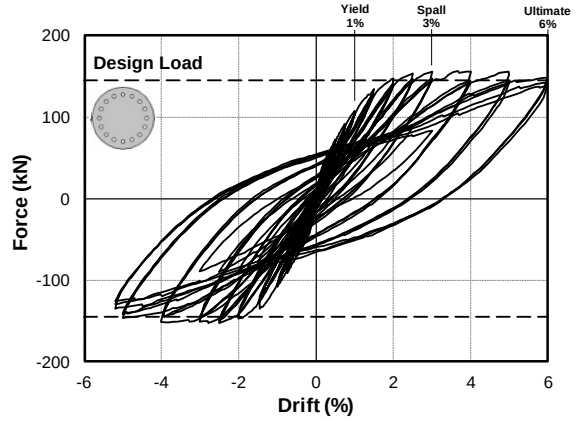

(a) HDC1

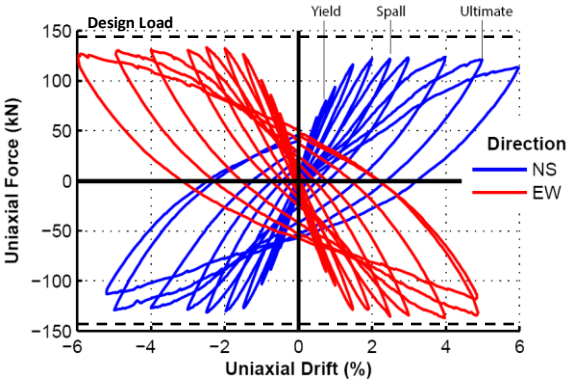

(b) HDC2 (uniaxial)

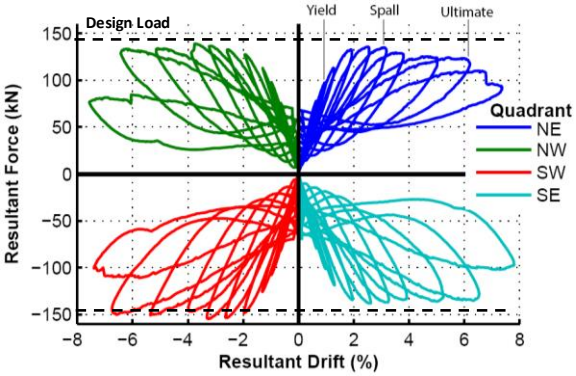

(c) HDC2 (resultant biaxial)

Figure 18. Force-Drift hysteresis plots for HDC1 and HDC2.

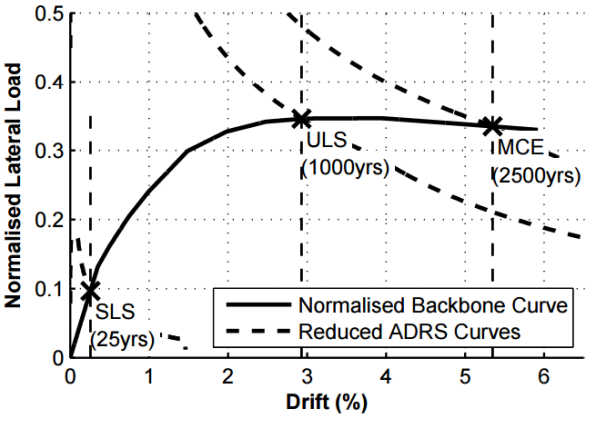

(a) HDC1 (North/South Direction)

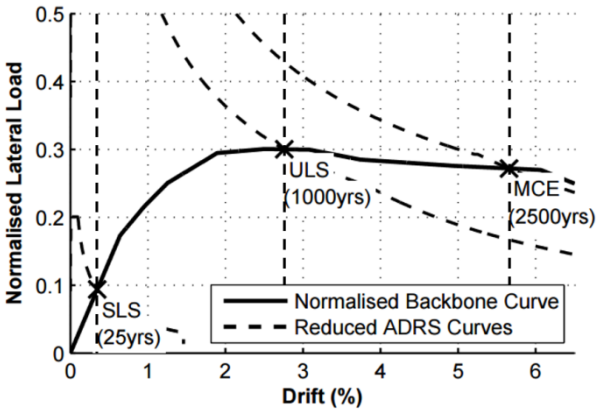

(b) HDC2 (North/South Direction)

Figure 19. ADRS curves for HDC1 and HDC2.

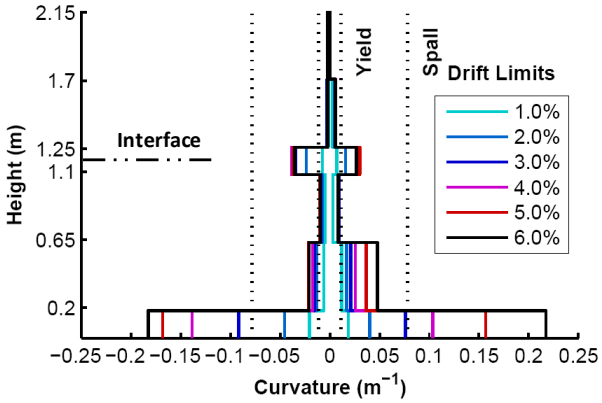

(a) HDC1 (North/South Direction)

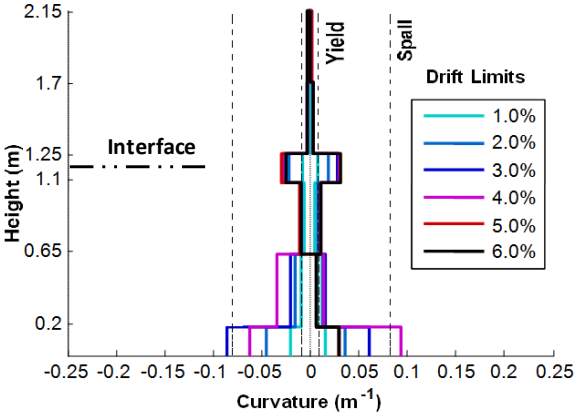

(b) HDC2 (North/South Direction)

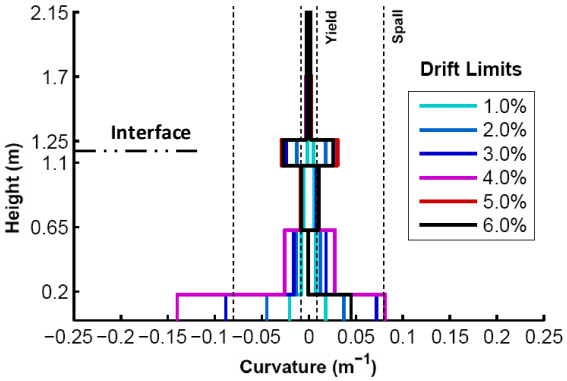

(c) HDC2 (East/West Direction)

Figure 20. Curvature distribution for HDC1 and HDC2.

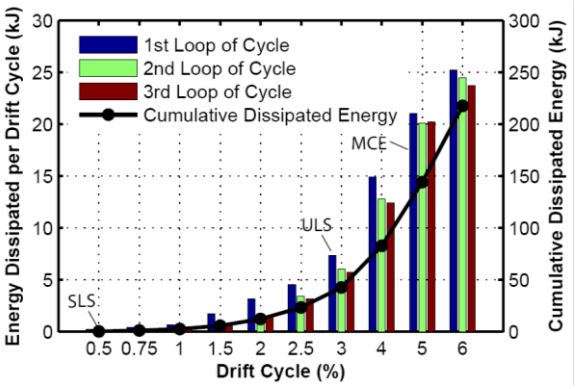

(a) HDC1

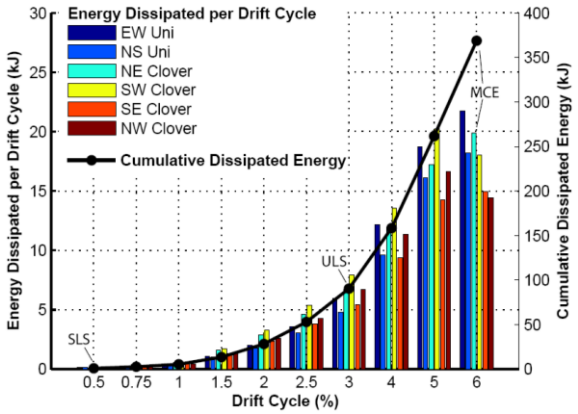

(b) HDC2

Figure 21. Dissipated energy for HDC1 and HDC2.

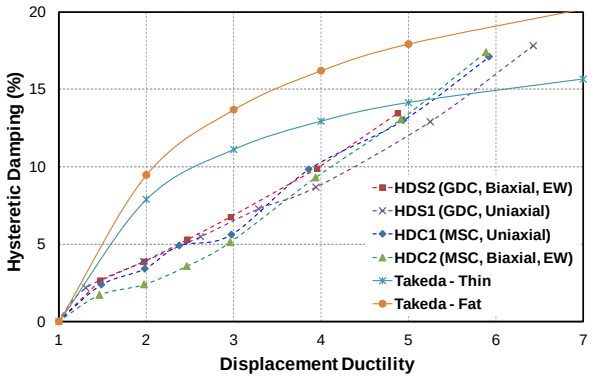

(a) Hysteretic damping plot

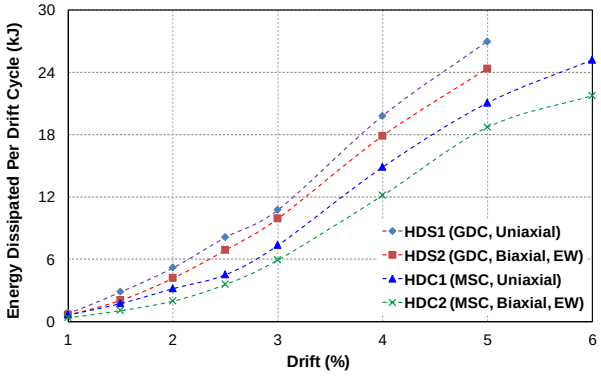

(b) Dissipated energy plot

Figure 22. Comparison of seismic performance for the four columns with GDC and MSC.

In Figure 22a, for all values of ductility, the specimens had lower values of hysteretic damping compared to that of a theoretical Takeda-Fat damping rule. In comparison to the theoretical Takeda-Thin damping rule, the specimens had lower values of hysteretic damping up to a ductility of around 5. Following that, HDS1, HDC1, and HDC2 had higher values of hysteretic damping.

Figure 22b presents a comparison of energy dissipation between the four columns in terms of increasing drift ratio.

Punching Shear (Pull Through) Testing: HDC1 and HDC2

Following testing of HDC1 and HDC2, punching shear (pull through) tests were carried out on the footings. The purpose of this was to demonstrate whether there was sufficient shear resistance left between the column stub and footing. The testing arrangement is shown in Figure 23a. A hydraulic actuator was used to load the column stub while holding down the footing with anchor bolts (Figure 23b).

During testing, radial cracking occurred in the footing which propagated from around the socket and extended to the perimeter of the footing (Figure 23c and Figure 23d). The axial load was increased to 3 times the ULS gravity load (1350 kN). There was no apparent slip of the column stub in the socket. This indicated that sufficient gravity capacity of the connection remained after cyclic loading with no substantial grout degradation.

CONCLUSIONS

In summary, ABC High Damage connections offer the potential for significant time savings during construction. Formation of plastic hinges, however, leads to structural damage which can result in costly repair, downtime in bridge functionality and residual deformation as observed following the Canterbury earthquakes. On important structures, bridge designers and owners should consider the use of non-emulative connection types to improve seismic performance as investigated in subsequent phases of this research project.

Appropriate connection detailing can, however, be used to improve the performance of High Damage connections such as those presented in this paper. Use of armouring and debonding of the starter bars can enhance the ductility of grouted duct connection. In HDS2, debonding of the starter bars was effective in distributing the inelastic deformation in the reinforcing bars. This reduced strain concentration effects at the column to footing interface which increased the displacement capacity of the column and helps to mitigate against low-cycle fatigue failure. In HDS2, bar rupturing occurred during the 7% resultant drift ratio cycle which is 30% higher than that of HDS1 (Figure 10).

For grouted duct connections, sufficient tolerance must be allowed for in the sizing of grouting ducts relative to the starter bars (approximately 20 mm). Member socket connection offers simpler assembly than grouted duct connection and larger construction tolerances.

In terms of seismic performance, the grouted duct connection showed a lower ultimate displacement capacity and a shorter plastic hinge length (approximately equal to half the section depth). On the other hand, the member socket connection showed a longer plastic hinge (approximately equal to the section depth) which increased the ultimate displacement and ductility capacities of the column. Figure 18a shows that HDC1 achieved a drift ratio of 6% in comparison to 5% which was achieved by HDS1 (Figure 10a). Also, Figure 18c indicates that HDC2 was able to achieve a resultant drift ratio under biaxial loading of nearly 8% while HDS2 (Figure 10c) could achieve only 6%. Further research is recommended to

quantify the plastic hinge length of the grouted duct and member socket connections.

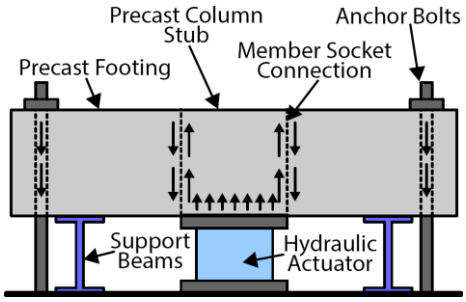

(a) Test setup

(b) Loading hydraulic jack

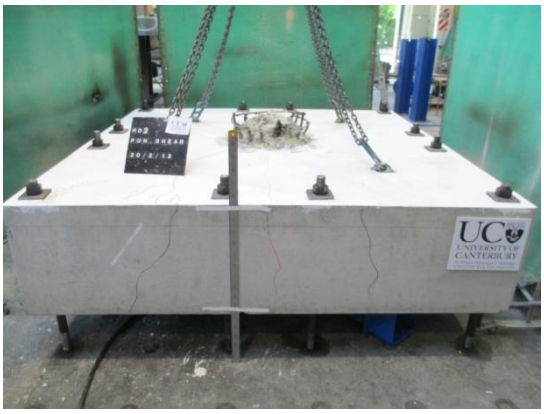

(c) Footing under testing

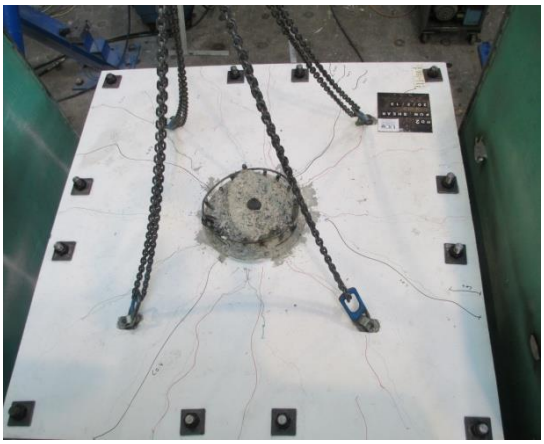

(d) Radial cracking of footing

Figure 23. Punching shear test setup for footing with MSC.

Both grouted duct and member socket connections for column-footing connections showed promising results with good energy dissipation and ductility. All four columns achieved the assumed design ductility of $\mu = 3$ at ULS performance level. Good strength and ductility characteristics of these connections indicate suitability for use in regions of moderate to high seismicity.

ACKNOWLEDGMENT

The authors would like to thank the New Zealand Ministry of Science and Innovation - Natural Hazards Research Platform for supporting this research as part of the project "Advanced Bridge Construction and Design for New Zealand" (ABCD). The project was coordinated at the University of Canterbury (2011-2015) by Associate Professor Alessandro Palermo. The authors express their gratitude to technicians Gavin Keats and Russell McConchie for helping with the testing.

REFERENCES

1 Palermo A and Mashal M (2012). "Accelerated Bridge Construction and Seismic Damage Resistant Technology: A New Zealand Challenge". *Bulletin of the New Zealand Society for Earthquake Engineering*, **45**(3): 123-134.

2 Billington SL, Barnes RW and Breen J E (1999). "A Precast Segmental Substructure System for Standard Bridges". *Journal of Precast/Prestressed Concrete Institute*, **44**(4): 56-73.

3 Ralls ML, Hyzak MD, Medlock RD and Wolf LM (2004). "Prefabricated Bridges - Current U.S. Practice and Issues". *Proceedings of FHWA/AASHTO Second National Prefabricated Bridge Elements and Systems Workshop*, New Jersey.

4 Khaleghi B (2010). "Washington State Department of Transportation Plan for Accelerated Bridge Construction". *Journal of the Transportation Research Board*, **2200**(1): 3-11.

5 Burkett WR., Nash PT, Bai Y, Hays C and Jones C (2004). "*Rapid Bridge Replacement Techniques"*. TechMRT Report No. 04568-1, Texas Tech University, Lubbock, Texas.

6 Utah Department of Transportation (2008). "*Accelerated Bridge Construction Standards Workshop"*. Utah Department of Transportation, Salt Lake City, Utah, United States.

7 Stanton, JF, Hawkins NM and Eberhard MO (1992). "Seismic Connections for Precast Concrete Structures". *Proceedings of 10th World Conference on Earthquake Engineering*, Madrid, Spain, 4403-4408.

8 Buckle IG (1994). *"The Northridge, California Earthquake of January 17, 1994: Performance of Highway Bridges"*. NCEER Technical Report No. 0008, University at Buffalo, New York, United States.

9 Hawkins N, Wood S and Stanton J (1994). "Performance Of Parking Garages In the 1994 Northridge Earthquake". *Proceedings of 13th American Society of Civil Engineers Structures Congress*, Boston, Massachusetts, United States.

10 Mander J and Cheng CT (1997). *"Seismic Resistance of Bridge Piers Based on Damage Avoidance Design"*. Technical Report NCEER-97-0014, University at Buffalo, New York, United States.

11 Marsh ML, Wenli M, Garrett BE, Stanton JF, Eberhard MO and Weinert MD (2011). *"Application of Accelerated Bridge Construction Connections in Moderate-to-High Seismic Regions"*. National Cooperative Highway

Research Program Report 698, Transportation Research Board, Washington D.C., United States.

12 Paulson C and Hanson, JM (1991). *"Fatigue Behaviour of Welded and Mechanical Splices in Reinforcing Steel"*. National Cooperative Highway Research Program Project 10-35 Final Report, Transportation Research Board, Washington D.C., United States.

13 Culmo M (2009). "*Connection Details for Prefabricated Bridge Elements and Systems"*. Report No. FHWA-IF-09-010, Federal Highway Agency, Office of Bridge Technology, Washington D.C., United States.

14 Matsumoto EE, Waggoner MC, Sumen G, Kreger ME, Wood SL and Breen JE (2001). *"Development of a Precast Bent Cap System"*. Report 1748-2, CTR, University of Texas at Austin, Texas, United States.

15 Matsumoto EE (2009). *"Emulative Precast Bent Cap Connections for Seismic Regions: Grouted Duct and Cap Pocket Test Results"*. Report ECS-CSUS-2009-05, California State University, Sacramento, California, United States.

16 Brenes F, Wood S and Kreger M (2006). *"Anchorage Requirements for Grouted Vertical-Duct Connectors in Precast Bent Cap Systems"*. Report No. 0-4176-S, CTR, University of Texas at Austin, Texas, United States.

17 Haraladsson O, Stanton JF and Eberhard MO (2011). *"Laboratory Tests of Column-to-Footing Socket Connections"*. Report No. FHWA-HIF-13-039, FHWA, Washington D.C., United States.

18 Hewes JT and Priestley MJN (2002). *"Seismic Design and Performance of Precast Concrete Segmental Bridge Columns"*. Report No. SSRP-2001/25, California Department of Transportation, Sacramento, California, United States.

19 Billington SL and Yoon JK (2004). "Cyclic Response of Unbonded Post-Tensioned Precast Columns with Ductile Fiber-Reinforced Concrete". *Journal of Bridge Engineering*, **9**(4): 353-363.

20 Palermo A (2004). *"The Use of Controlled Rocking in the Seismic Design of Bridges"*. PhD Dissertation, Politecnico di Milano, Milan, Italy, 277 pp.

21 Stanton JF, Wacker JM, Hieber DG and Eberhard MO (2005). *"Design of Precast Concrete Pier for Rapid Bridge Construction in Seismic Regions"*. Report No. WA-RD 611.1, Washington Department of Transportation, Olympia, Washington, United States.

22 Palermo A and Pampanin S (2008). "Enhanced Seismic Performance of Hybrid Bridge Systems: Comparison With Traditional Monolithic Solutions". *Journal of Earthquake Engineering*, **12**: 1267-1295.

23 Saiidi MS and Wang H (2006). "Exploratory study of seismic response of concrete columns with shape memory alloys reinforcements". *American Concrete Institute Structural Journal*, **103**(3): 435-442.

24 White S and Palermo A (2014). "Controlled Damage Precast Connections for Accelerated Bridge Construction in Regions of High Seismicity". *Proceedings of New Zealand Society for Earthquake Engineering Conference*, Auckland, New Zealand.

25 Mashal M and Palermo A (2014). "Quasi-Static Experimental Testing of Emulative and Low Damage Seismic Technologies for ABC in Seismic Areas". *Proceedings of National Accelerated Bridge Construction Conference*, Miami, Florida, United States.

26 New Zealand Transportation Agency (2008). "*Standard Precast Concrete Bridge Beams*". Report No. NZTA 364, New Zealand Transportation Agency, Wellington, 57 pp.

27 New Zealand Transportation Agency (2003). "*Bridge Manual 2nd Edition*". New Zealand Transportation Agency, Wellington, New Zealand.

28 Standards New Zealand (2004). "*NZS1170.5: Structural Design Actions. Part 5: Earthquake Actions-New Zealand*". Standards New Zealand, Wellington, 55 pp.

29 American Concrete Institute (2001). *"Acceptance Criteria for Moment Frames Based on Structural Testing"*. Report No. ACI T1.1-01, Farmington Hills, Michigan, United States.

30 Marriott D (2009). "*The Development of High-Performance Post-Tensioned Rocking Systems for the Seismic Design of Structures*". PhD Dissertation, University of Canterbury, Christchurch, New Zealand, 556 pp.

31 Muir CA, Pampanin S and Bull DK (2011). "Preliminary Observations from Biaxial Testing of a Two-storey, Two-by-One Bay, Reinforced Concrete Slotted Beam Superassembly". *Proceedings of New Zealand Society for Earthquake Engineering Conference*, Christchurch, New Zealand.

32 Riva P (2006). "Seismic Behaviour of Precast Column-To-Foundation Grouted Sleeve Connections". *Proceedings of International Conference on Advances in Engineering Structures*, Ontario, Canada, 121-128.

33 Restrepo JI, Tobolski MJ, and Matsumoto EE (2011). *"Development of a Precast Bent Cap System for Seismic Region"*. National Cooperative Highway Research Program *Report 681*, Transportation Research Board, Washington D.C., United States.

34 Standards New Zealand (2004). "*NZS3101: Concrete Structures Standards Part 1: The Design of Concrete Structures*". Standards New Zealand, Wellington, 306 pp.

35 Mander JB, Priestley MJN and Park R (1988). *"*Theoretical Stress-Strain Model for Confined Concrete". *Journal of Structural Engineering*, **114**(8):1804-1826.

36 Raynor DJ, Lehman DE and Stanton JF (2002). "Bond-Slip Response of Reinforcing Bars Grouted In Ducts". *American Concrete Institute Structural Journal*, **99**(5).

37 Mander J, Panthaki F and Kasalanati A (1994). "Low-Cycle Fatigue Behaviour of Reinforcing Steel". *Journal of Materials in Civil Engineering*, **6**: 453-468.

38 Kawashima K, Hosoiri K, Shoji G and Sakai J (2001). Effect of Unbonding of Main Reinforcements at Plastic Hinge Region for Enhancing Ductility of Reinforced Concrete Bridge Columns". *Proceedings of Japan Society of Civil Engineers Conference*, 45-64.

39 Pampanin S, Marriot D and Palermo A (2010). "*PRESSS Design Handbook"*. New Zealand Concrete Society Inc., Auckland, 282pp.

40 Haraldsson OS, Janes TM, Eberhard MO and Stanton JF (2013). "Seismic Resistance of Socket Connection between Footing and Precast Column*"*. *Journal of Bridge Engineering*, **18**(9):910-919.

41 Osanai Y, Watanabe F and Okamoto S (1996). "Stress Transfer Mechanism of Socket Base Connections with Precast Concrete Columns". *American Concrete Institute Structural Journal*, **93** (3).

42 Dwairi HM., Kowalsky MJ and Nau JM (2007). "Equivalent Damping in Support of Direct Displacement-Based Design". *Journal of Earthquake Engineering*, **11**(4):512-530.

43 Priestley MJN, Calvi GM and Kowalsky MJ (2007). *"Displacement-Based Seismic Design of Structures"*. IUSS Press, Pavia, 721pp.